Inelastic stress-strain behaviour of cyclic loaded notched specimens

J.Olschewski
Bundesanstalt für Materialforschung und -prüfung (BAM), Berlin, FR Germany

1 INTRODUCTION

Inelastic constitutive theories are needed for an appropriate evaluation of the strength of high-temperature structures such as nuclear and non-nuclear power plant components, gasturbines and aerospace components and for developing adequate methods of life prediction. The representation of the inelastic mechanical response of structural materials used in this field is a difficult task. Under appropriate conditions the response is rate-insensitive, and thus rate-independent plasticity is adequate. However, experiments suggest that rate-dependence is often important. The rate-independent elastic-plastic material model commonly used in FE computer codes is based on the ORNL-guidelines (1974) uses the linear kinematic hardening rule. This model is incapable of representing both the transient hardening character and the rate-dependence of high-temperature materials. Therefore, several generalizations of the rate-independent elastic-plastic material model have been developed. In this paper FE calculations based on a model of combined isotropic and kinematic hardening of an initial Mises yield surface are discussed. The proposed model, which incorporates a realistic description of nonlinear transient cyclic hardening behaviour of the nickel based alloy PE 16 for a given strain rate, is applied in investigating the multi-axial stress-strain state in a circumferential notched cylindrical bar. The calculated notch stresses and strains are compared with those obtained by using a model with multilinear kinematic hardening and Masing behaviour. Special attention is focussed on the question, how the stress state at the notch root, represented in the space of principle stresses, varies due to cyclic loading.

2 MODELING OF CYCLIC STRESS-STRAIN BEHAVIOUR

As in the classical time independent plasticity theory the existence of a yield surface in stress space is assumed. Using the Von Mises criterium it can be written:

$$(1) \qquad f = \frac{1}{2}(\underset{\sim}{\sigma}' - \underset{\sim}{\alpha}') \cdot (\underset{\sim}{\sigma}' - \underset{\sim}{\alpha}') - \kappa^2(p) = 0,$$

where $\underset{\sim}{\sigma}'$ and $\underset{\sim}{\alpha}'$ are the stress and back stress deviators. The hardening behaviour is expressed by a set of a scalar and a tensorial internal variable. The scalar or isotropic internal variable κ is associated with the size of the yield surface and depends on the accumulated plastic

strain p, defined by

$$\dot{p} = \sqrt{\frac{2}{3}\,\dot{\underset{\sim}{\varepsilon}}^{p} \cdot \dot{\underset{\sim}{\varepsilon}}^{p}} \,. \tag{2}$$

The tensorial or kinematical internal variable $\underset{\sim}{\alpha}$ denotes the center of the yield surface.

The plastic strain rate $\dot{\underset{\sim}{\varepsilon}}^{p}$ follows the classical normality hypothesis:

$$\dot{\underset{\sim}{\varepsilon}}^{p} = \dot{\lambda}\,\frac{\partial f}{\partial \underset{\sim}{\sigma}} = \dot{\lambda}\,(\underset{\sim}{\sigma}' - \underset{\sim}{\alpha}') = \sqrt{\frac{3}{2}}\,\dot{p}\,\frac{\underset{\sim}{\sigma}' - \underset{\sim}{\alpha}'}{|\underset{\sim}{\sigma}' - \underset{\sim}{\alpha}'|} \,. \tag{3}$$

The hardening rules are given by evolution laws of the internal variables:

$$\dot{\underset{\sim}{\alpha}}' = c\,(p)\,\dot{\underset{\sim}{\varepsilon}}^{p} \,, \tag{4}$$

$$\dot{\kappa} = d\,(p)\,\dot{p} \,, \tag{5}$$

which are similar to those proposed by Eisenberg & Phillips (1968).

The isotropic hardening behaviour is based on the assumption that after a transient hardening process a stabilized cycle is reached. Conditions necessary to generate a stable hysteresis loop are:

$$\text{(6)} \qquad \text{i)} \quad \kappa \to \kappa_S \,, \qquad \text{ii)} \quad d \to 0 \,,$$

with increasing number of cycles. κ_S is the saturation value of κ. These conditions are fulfilled with

$$\text{(7)} \qquad \kappa = \kappa_S + (\kappa_0 - \kappa_S)e^{-bp}, \qquad \kappa(0) = \kappa_0$$

or by

$$\dot{\kappa} = -b(\kappa_0 - \kappa_S)e^{-bp}\,\dot{p} = b(\kappa_S - \kappa)\,\dot{p} \,.$$

The coefficients κ_0, κ_S and b are temperature- and strain rate-dependent. The variation of κ with the accummulated plastic strain p is shown for the alloy PE 16 (Kutumbarao 1986) in Figure 1. Analyzing these experimental data one gets for Θ = 650 °C and $\dot{\varepsilon} = 4 \cdot 10^{-3}\,s^{-1}$:

$$\kappa_0 = 267 \text{ MPa}, \quad \kappa_S = 393 \text{ MPa}, \quad b = 18.4.$$

The kinematic hardening effect corresponds to the translational movement of the yield surface in stress space. The most commonly used kinematic hardening rule is the linear rule due to Prager (1955). This rule implies a linear relationship between stresses and strains in the plastic range if $\kappa = \kappa_0$ during plastic cycling. A generalization like the Mroz's model (1967) based on a piecewise linear approximation of the stress curve and the property of the Masing rule gives a better description of the hysteresis loop but is unable to describe the transient hardening behaviour from the initial state to the saturation state.

To develop a kinematic model which gives the shape of the hysteresis loop one has to compare the isotropic and kinematic hardening rules with

the cyclic stress-strain behaviour of the material, for example given by a variable plastic hardening modulus:

$$E_p = \frac{d\sigma}{d\varepsilon^p} = \frac{3}{2}\left(c(p) - \frac{2}{\sqrt{3}}\, d(p)\right). \tag{9}$$

Using a Ramgerg-Osgood approximation for the stress-strain relationship of the material

$$\varepsilon = \frac{\sigma}{E} + \left(\frac{\sigma}{\sigma_R}\right)^{\frac{1}{m}}, \tag{10}$$

E_p can continously expressed by the accumulated plastic strain p:

$$E_p = m\sigma_R\, p^{m-1}. \tag{11}$$

The parameters σ_R and m are temperature- and strain-rate-dependent and furthermore, they vary with cyclic straining. From (9) and (11) it follows for the material function c(p):

$$\begin{aligned} c(p) &= \frac{2}{3} E_p + \frac{2}{\sqrt{3}}\, d(p) \\ &= \frac{2}{3}\, m\sigma_R\, p^{m-1} - \frac{2}{\sqrt{3}}\, b(\kappa_o - \kappa_s)e^{-bp}. \end{aligned} \tag{12}$$

With this the plastic multiplier $\dot{\lambda}$ in (3) is obtained using the consistency condition, i. e. that plastic flow occurs only if $\dot{f} = 0$:

$$\dot{\lambda} = \frac{2G\,(\underset{\sim}{\sigma}' - \underset{\sim}{\alpha}') \cdot \dot{\underset{\sim}{\varepsilon}}}{\kappa^2\left(4G + 2c(p) + \frac{4}{\sqrt{3}}\, d(p)\right)} \tag{13}$$

where G is the shear modulus and $\dot{\underset{\sim}{\varepsilon}}$ the total strain rate given as the sum of an elastic and a plastic part.

In generalizing this model for describing cyclic hardening the variation of the parameter σ_R and m with increasing number of cycles has to be taken into account. For that purpose an assumption very similar to (7) is also used for σ_R and m

$$\sigma_R = \sigma_{Rs} + (\sigma_{Ro} - \sigma_{Rs})e^{-b_1 p}, \tag{14}$$

$$m = m_s + (m_o - m_s)e^{-b_2 p}. \tag{15}$$

The parameters b_1 and b_2 are suitable determined to get a good representation of the transient hardening behaviour. For the alloy PE 16 at Θ = 650 °C and $\dot{\varepsilon} = 4 \cdot 10^{-3}\,s^{-1}$ the following parameter are obtained from strain-controlled low cycle fatigue tests (Kutumbarao 1986):

$m_o = 0.135$, $m_s = 0.054$, $\sigma_{Ro} = 1153$ MPa, $\sigma_{Rs} = 2125$ MPa,
$b_1 = 52.6$, $b_2 = 23.3$.

3. APPLICATION ON A NOTCHED SPECIMEN

As an example a circumferential notched cylindrical bar has been analysed. The finite element idealization is given in Figure 2. 70 axisymmetric 8-noded elements giving rise to 462 degrees of freedom. The proposed material models are incorporated in the FE program ADINA (1984).

At first the behaviour of the proposed material model has been examined in comparing the FE results obtained from a FE model of a smooth axisym-

metric specimen under uniaxial tension-compression loading (strain amplitude: $\varepsilon_a = 0.026$) with corresponding experimental results. The comparison is made in Figure 3. It is shown that the examined material model gives a adequate accuracy in predicting the hysteresis loops under uniaxial loading conditions.

Since all our structural components contain stress and strain concentrators as, for example notches, it is more important to study the behaviour of notched specimens. But, unfortunately, the experimental techniques are not developed to measure the strain state at the notch root at high temperatures. Therefore, as yet we are not able to compare the FE results with experimental data, but we hope to overcome these experimental difficulties in the future.

From that reason a comparison can be made only on the basis of material models. Figure 4 shows the hysteresis loops obtained by using a material model based on a multilinear kinematic hardening. The isotropic hardening aspect is neglected, i. e. this model is a multilinear generalization of that recommended by the ORNL (1974) guidelines. Figure 4 shows the the influence of the material data used in the FE calculation. The stress amplitude increases by using a cyclic stabilized stress-strain curve, because of the cyclic hardening behaviour of PE 16.

The hysteresis loops shown in Figure 5 are determined from the notch opening stress and strain calculated by using the proposed material model with a combination of isotropic and kinematic hardening. The notched specimen is subjected to a strain-controlled LCF-loading (strain amplitude $\varepsilon_a = 0.02$). One can observe that in a uniaxially stressed notched cylindrical bar the qualitative response of the material element at the notch root is similar to the response of a smooth bar. Figure 6 shows the corresponding variation of the equivalent stress and strain at the notch root.

The stress and strain distribution ahead of the crack tip in the ligament is shown in Figures 7 and 8. It is seen that the stress maximum lying ahead of the crack tip increases with increasing number of cycles. In this Figures the stress and strain distributions for the first three cycles are shown. After a few cycles a saturation state is reached. In Figure 9 a comparison is made in the stress distributions of the saturation cycle for the two examined material models. The maximum of the notch opening stress calculated by using the nonlinear hardening model is considerably higher than that using the multilinear hardening model.

Figures 10 and 11 show the varying stress states of the notch root due to uniaxial cyclic loading in the space of principle stresses. It is seen that the stress states are strongly influenced by the hardening rules used and furthermore, that there is by no means a proportional loading behaviour in the inelastic regime. Therefore, the question arises regarding the limitations of the concept of smooth specimen simulation.

REFERENCES

ADINA 1984. A finite element program for automatic dynamic incremental analysis. Report AE 84-1. Watertown: ADINA Eng. Inc.

Corum, J. M. et al. 1974. Interim Guidelines for detailed inelastic analysis of high-temperature reactor system components. ORNL-5014.

Eisenberg, M. A. & A. Phillips 1968. On nonlinear kinematic hardening. Acta Mechanica 5: 1 - 13.

Kutumbarao, V. V. 1986. Private communication.

Mróz, Z. 1967. On the description of anisotropic work hardening. J. Mech. Phys. Solids 15 (3): 163 - 175.

Prager, W. 1955. The theory of plasticity: A survey of recent achievements. Proc. of the Inst. of Mech. Engineers (London) 169: 41 - 50.

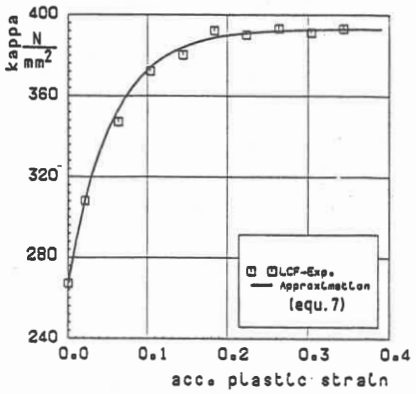

Figure 1. Isotropic hardening variable κ vs acc. plastic strain.

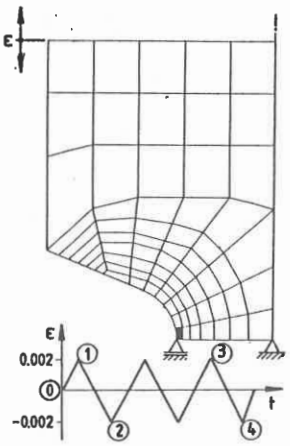

Figure 2. FE mesh, axisymmetric, strain controlled loading notch radius ρ = 0.25 mm, K_t = 3.2.

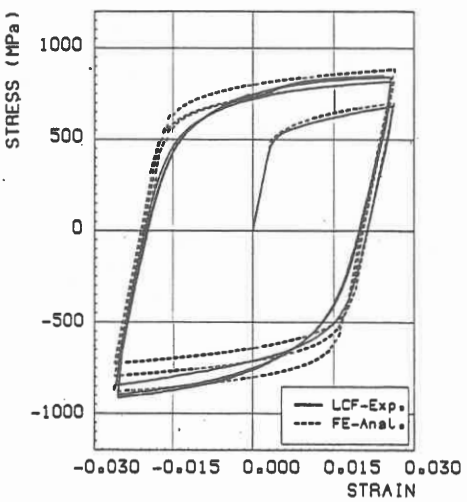

Figure 3. Comparison of experimental data (PE16: Θ = 650 C, $\dot{\varepsilon}$ = 4 $10^{-3}s^{-1}$, ε = 0.026) with prediction based on nonlinear hardening model.

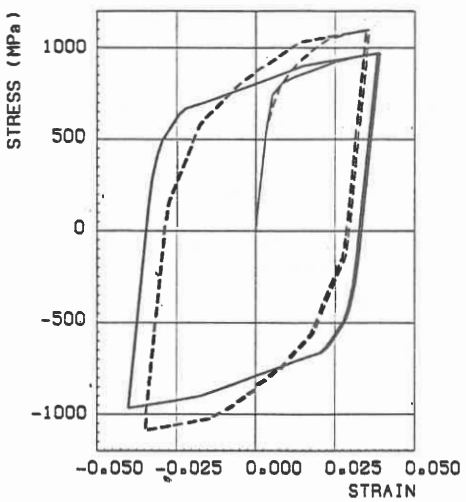

Figure 4. Notch stress vs notch strain, multinear hardening model with Masing behaviour:
---- monotonic σ-ε - curve
---- cyclic stab. σ-ε - curve

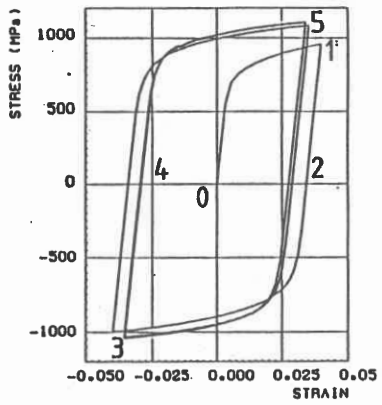

Figure 5. Notch stress vs notch strain, nonlinear hardening model.

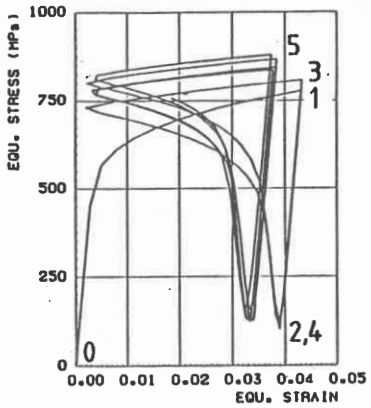

Figure 6. Equivalent stress vs equivalent strain at the notch root, nonlinear hardening model.

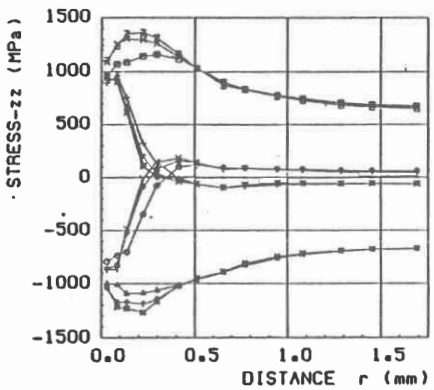

Figure 7. Notch opening stress ahead of the notch root, 3 cycles, nonlinear hardening model.

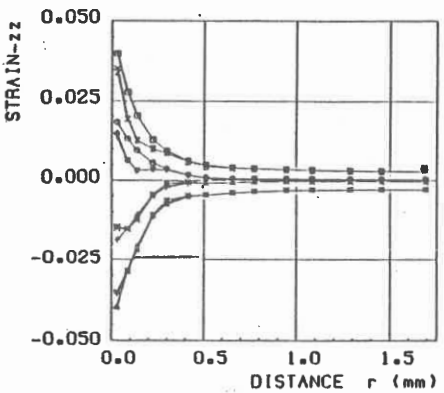

Figure 8. Notch opening strain ahead of the notch root, 3 cycles, nonlinear hardening model.

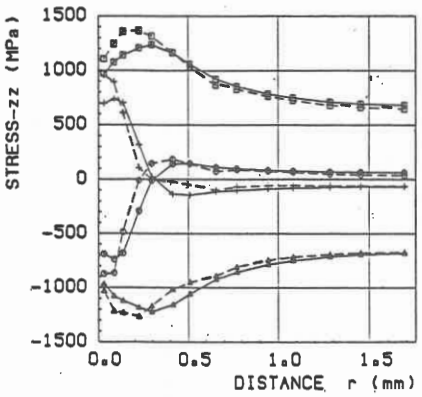

Figure 9. Comparison of the notch opening stress ahead of the notch root at saturation cycle:
---- multilinear hardening
---- nonlinear hardening

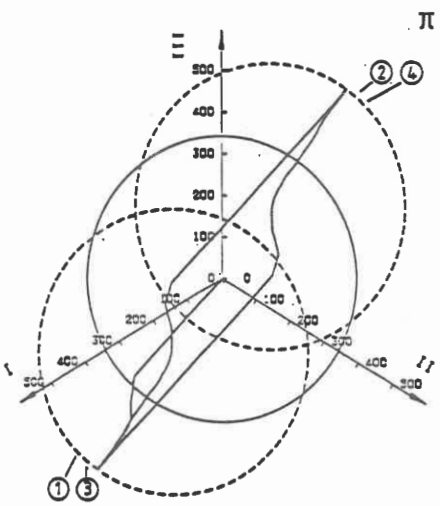

Figure 10. Variation of the multiaxial stress state at the notch root in the space of principle stresses, multilinear hardening, Masing behaviour.

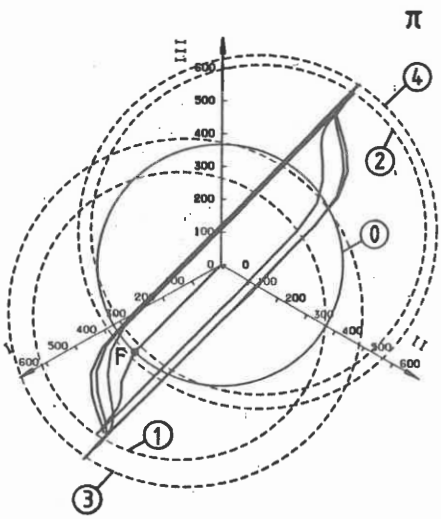

Figure 11. Variation of the multiaxial stress state at the notch root in the space of principle stresses, nonlinear hardening model.